



Effects of substrate temperature on the structure and luminescence of transparent red-emitting Eu-doped Y_2O_3 thin films

Do Hyeong Kim¹ · Joo Han Kim¹

Received: 15 October 2021 / Revised: 26 November 2021 / Accepted: 30 November 2021 / Published online: 18 January 2022
© The Korean Physical Society 2022

Abstract

Transparent red-emitting Eu-doped Y_2O_3 thin films were deposited by radio frequency magnetron sputtering and the effects of substrate temperature on their structure and luminescence were investigated. X-ray photoelectron spectroscopy measurements showed that the stoichiometric Y_2O_3 was formed and the Eu ions were incorporated mainly in the form of Eu^{3+} in the films. The $Y_2O_3:Eu$ films had a mixed crystalline structure consisting of monoclinic and cubic phases at low substrate temperatures. A single phase of cubic structure was obtained at substrate temperatures above 300 °C and the films were preferentially oriented along the [111] direction. The $Y_2O_3:Eu$ films deposited at room temperature were under residual compressive strain, which was decreased with increasing substrate temperature. The $Y_2O_3:Eu$ films showed the photoluminescence with the most intense peak at 613 nm which originated from the transition between the 5D_0 and 7F_2 states in Eu^{3+} ions. The PL intensity was increased and the spectral linewidth was decreased with increasing substrate temperature. All the $Y_2O_3:Eu$ films showed good transparency with an optical transmittance greater than 80% in the wavelength region from 400 to 1100 nm. The transmittance of the $Y_2O_3:Eu$ films was decreased as the substrate temperature increased, which was due to the increased surface roughness of the films.

Keywords Yttrium sesquioxide · Substrate temperature · Transmittance · Structural properties

1 Introduction

Thin films of yttrium sesquioxide doped with europium ($Y_2O_3:Eu$) have attracted much attention in the areas of display technologies. This is because $Y_2O_3:Eu$ is a preeminent red-emitting luminescent material with a high luminescence quantum yield [1–3]. $Y_2O_3:Eu$ can be prepared in the form of thin films and powders. It is advantageous to use $Y_2O_3:Eu$ in thin-film form because it offers several benefits compared to its powder form [4–6]. Thin-film $Y_2O_3:Eu$ exhibits a smooth surface with uniform thickness and dense structure. This enables to make smaller pixel sizes and allows a higher resolution display screen. In addition, thin-film $Y_2O_3:Eu$ is well adhered to a substrate and shows high thermal stability.

Another advantageous property of thin-film $Y_2O_3:Eu$ is optical transparency. Thin-film $Y_2O_3:Eu$ has a smooth surface which leads to low light scattering and high transparency. Transparent display panels can be fabricated using transparent luminescent thin films. Organic light emitting diodes (OLEDs) are usually applied to make a transparent display. However, OLEDs suffer from degradation issues because organic materials are extremely sensitive to moisture and oxygen [7, 8]. Organic materials used in OLEDs also have drawbacks of low thermal stability and mechanical strength [8, 9]. Robust transparent displays can be made using $Y_2O_3:Eu$ because it is much more thermally and chemically stable and mechanically stronger than organic materials. A recent study showed that transparent electroluminescent display devices can be fabricated using an $Y_2O_3:Eu$ -based multilayer structure [10].

Thin-film $Y_2O_3:Eu$ can be prepared by a wide range of thin-film deposition techniques, such as spray pyrolysis [4], electron beam evaporation [5], atomic layer deposition [10], sputtering [11], electrodeposition [12], metal–organic chemical vapor deposition (MOCVD) [13], electrostatic-assisted

✉ Joo Han Kim
jooahan@cbnu.ac.kr

¹ Department of Advanced Materials Engineering, Chungbuk National University, Cheongju 28644, Korea

CVD [14], pulsed laser ablation [15], and sol–gel process [6]. Among them, the sputtering technique has advantages, such as simple processing structure and in-line manufacturing capabilities. For sputter deposition of thin films, substrate temperature is of critical importance in obtaining high-quality thin films. Therefore, we investigated the effects of substrate temperature on the properties of $Y_2O_3:Eu$ films prepared by sputtering. The correlations of the photoluminescent emission and optical transmittance with the crystalline structure and surface morphology of the $Y_2O_3:Eu$ films were examined.

2 Experiments

Thin-film $Y_2O_3:Eu$ was deposited using a radio frequency (RF) magnetron sputtering technique. Sputtering was carried out on sapphire (0001) substrates using an Eu-doped Y_2O_3 target in an Ar gas atmosphere. Prior to deposition of the films, the sputtering chamber was pumped by a turbomolecular pump until a base pressure of less than 1×10^{-6} Torr was achieved. The deposition was performed in the substrate temperature range from room temperature (25 °C) to 600 °C. The gas pressure and the RF power density were held at 2×10^{-2} Torr and 5.92 Wcm^{-2} , respectively, during deposition.

The chemistry of the $Y_2O_3:Eu$ films was examined by X-ray photoelectron spectroscopy (XPS, Ulvac Phi) using Al K_{α} radiation. The crystalline quality of the $Y_2O_3:Eu$ films was investigated by X-ray diffraction (XRD), which was performed using a SmartLab Rigaku diffractometer with Cu K_{α} radiation. The XRD patterns were collected in the 10–80° 2 θ range. The phases were identified by comparing experimental data with those from the Joint Committee on Powder Diffraction Standards (JCPDS) database. The surface morphology of the $Y_2O_3:Eu$ films was examined by atomic force microscopy (AFM) with a Bruker Dimension Icon. The photoluminescence (PL) emission spectra of the $Y_2O_3:Eu$ films were measured using a Perkin Elmer LS 55 spectrometer. The PL spectra were measured after excitation at a wavelength of 207 nm. The optical transmittance spectra of the $Y_2O_3:Eu$ films were measured using a Perkin Elmer Lambda 35 spectrophotometer in the range of 190–1100 nm.

3 Results and discussion

Figure 1 shows the survey scan spectra of X-ray photoelectron spectroscopy for the $Y_2O_3:Eu$ films deposited at different substrate temperatures. The spectra were collected before and after surface etching by Ar^+ ion beam etching for 3 min at 3 keV. It can be found that all the films mainly contained Y, O, and Eu elements. As shown in Fig. 1a, before surface

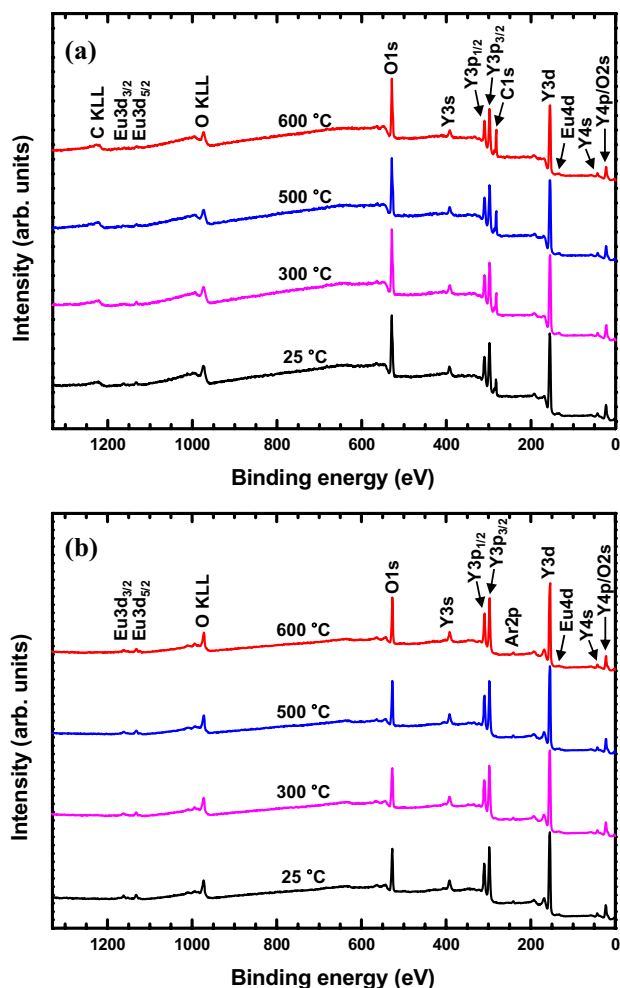


Fig. 1 XPS survey spectra of the $Y_2O_3:Eu$ films deposited at different substrate temperatures. The spectra were measured **a** before and **b** after surface etching

etching, C 1s and C KLL Auger peaks were detected due to the surface contamination from ambient exposure. As seen in Fig. 1b, the C 1s and C KLL Auger peaks disappeared, indicating that the contaminated carbon on the surface was completely eliminated after surface etching. The Ar 2p signal appeared, revealing that Ar was implanted by Ar^+ ion beam etching.

Figure 2 shows the XPS core level spectra of C 1s, Y 3d, O 1s, and Eu 4d regions for the $Y_2O_3:Eu$ films deposited at 600 °C. Figure 2a, c, e, and g are the spectra obtained before surface etching. Figure 2b, d, f, and h are the spectra obtained after surface etching. As shown in Fig. 2a, the C 1s peak was deconvoluted into three components. The main component with binding energy at 284.8 eV can be identified as C–C bond. The other two components centered at 285.93 and 289.23 eV correspond to C–O–C and O=C=O bonds, respectively. As can be seen in Fig. 2b, these carbon contamination peaks were completely removed by surface

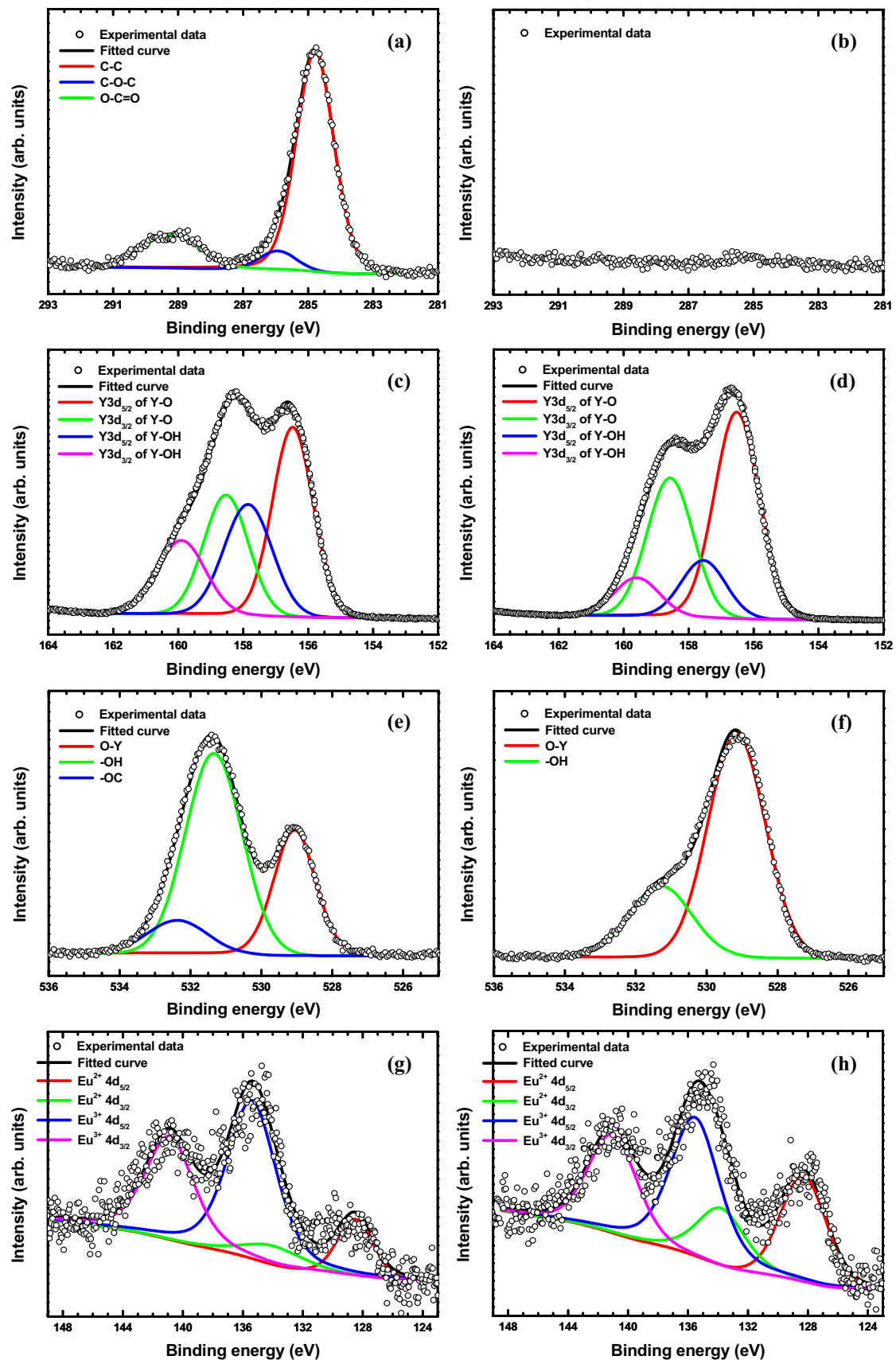


Fig. 2 XPS core level spectra of **a** and **b** C1s, **c** and **d** Y3d, **e** and **f** O1s, and **g** and **h** Eu4d regions for the $\text{Y}_2\text{O}_3:\text{Eu}$ films deposited at 600°C

etching. Figure 2c and d show the Y 3d spectra before and after surface etching, respectively. The Y 3d peak shows two pairs of components, which can be identified by two different spin–orbit doublets. The first pair of the Y 3d_{5/2} and 3d_{3/2} components with binding energies at 156.50 ± 0.02 and 158.55 ± 0.02 eV, respectively, is assigned to Y–O bond [16], showing that the stoichiometric Y₂O₃ was formed. The second pair of the Y 3d_{5/2} and 3d_{3/2} components appears at 157.70 ± 0.16 and 159.75 ± 0.16 eV, respectively, which is assigned to hydroxylated Y–OH bond caused by atmospheric moisture. After surface etching, as shown in Fig. 2d, the Y–OH components are still detectable although their intensities are reduced. This is because the hydroxylated Y₂O₃ is easily formed due to hygroscopic nature of Y₂O₃ [17].

Figure 2e and f show the O 1s spectra before and after surface etching, respectively. As shown in Fig. 2e, before surface etching, the O 1s peak shows three components. The component located at 529.11 ± 0.05 eV corresponds to O–Y bond [16], showing the presence of stoichiometric Y₂O₃, which is consistent with the Y 3d spectra analysis. The component at 531.31 ± 0.03 eV originates from hydroxyl groups [18]. The component at 532.36 eV is related to the oxygen bonded to carbon [19]. After surface etching, as shown in Fig. 2f, the intensity of the component from hydroxyl groups decreased. The component from the oxygen bonded to carbon disappeared, indicating that the contaminated carbon was removed by surface etching. Figure 2g and h show the Eu 4d spectra before and after surface etching, respectively. The Eu 4d peak can be deconvoluted into two pairs of spin–orbit doublets. The doublet peaks located at 135.46 ± 0.07 and 140.96 ± 0.07 eV can be ascribed to the 4d_{5/2} and 4d_{3/2} binding energies, respectively, from Eu³⁺ ions. Another doublet peaks located at 128.4 ± 0.1 and 133.9 ± 0.1 eV correspond to the Eu²⁺ 4d_{5/2} and Eu²⁺ 4d_{3/2}, respectively. The intensities of Eu³⁺ peaks are higher than Eu²⁺ peaks, showing that Eu ions were mainly in the form of Eu³⁺ in the films. The intensities of Eu²⁺ peaks increased after surface etching, which resulted from preferential removal of oxygen by Ar⁺ ion beam sputtering.

Figure 3 shows the PL emission spectra of the Y₂O₃:Eu films deposited at temperatures between 200 and 600 °C. No PL emission was observed from the films deposited at room temperature. The PL spectra consist of a series of emission peaks originating from the transitions of Eu³⁺ ions. All the emission peaks are attributed to the transitions from the ⁵D₁ and ⁵D₀ excited states to the ⁷F_J ground state. The most intense peak is located at 613 nm which is from the ⁵D₀ to ⁷F₂ transition, as labeled in Fig. 3. These PL spectra, together with the XPS spectra, clearly show that the Eu ions were incorporated mainly in the form of Eu³⁺ in the films. Figure 4 shows the intensity and the spectral linewidth for the PL emission at 613 nm as a function of substrate

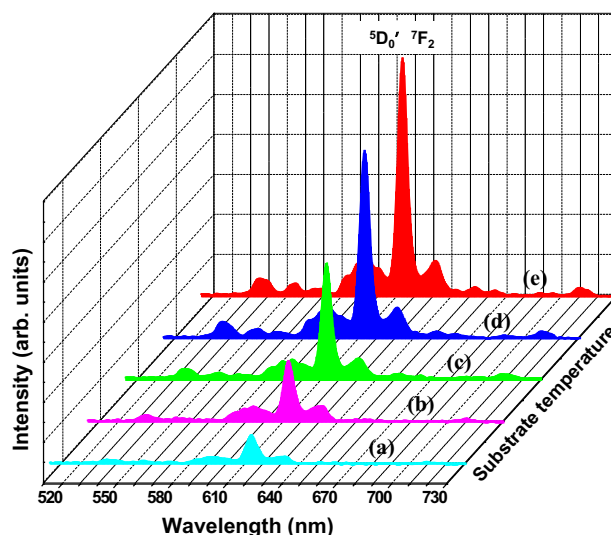


Fig. 3 PL emission spectra of the Y₂O₃:Eu films deposited at a 200, b 300, c 400, d 500, and e 600 °C

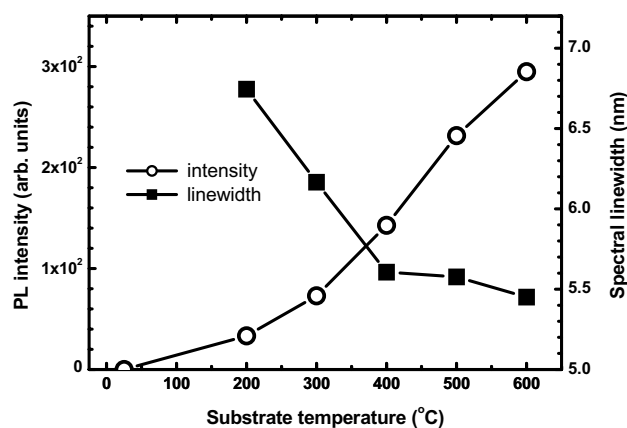


Fig. 4 PL intensity and spectral linewidth as a function of substrate temperature

temperature. The spectral linewidth was measured as the full width at half maximum of the PL emission peak at 613 nm. As can be seen in Fig. 4, the PL intensity was increased and the spectral linewidth was decreased with increasing substrate temperature. As will be explained below, this is attributed to the improved crystalline quality and the increased surface roughness of the films.

Figure 5 shows the XRD patterns of the Y₂O₃:Eu films deposited at different substrate temperatures. The films deposited at room temperature show the peaks corresponding to monoclinic and cubic Y₂O₃ phases. The diffraction peaks from the cubic phase are marked with Miller indices [20]. The peaks marked with the symbol (▼) correspond to the monoclinic phase [21]. These diffraction peaks show that the films deposited at room temperature had a mixed

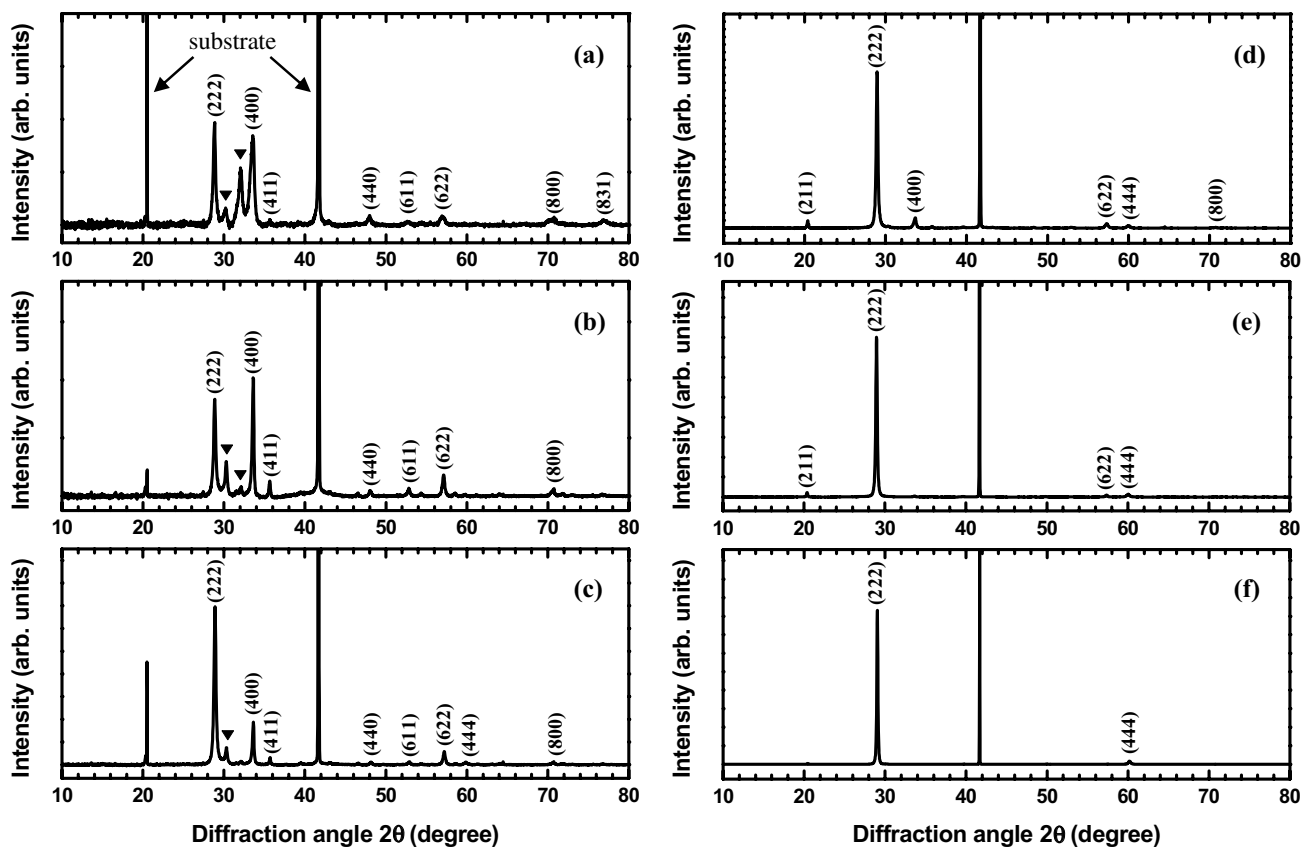


Fig. 5 XRD patterns of the $Y_2O_3:Eu$ films deposited at a 25, b 200, c 300, d 400, e 500, and f 600 °C

crystalline structure consisting of monoclinic and cubic phases. Y_2O_3 typically crystallizes in a thermodynamically stable cubic structure. However, it is known that the monoclinic structure of Y_2O_3 could also be formed when the Y_2O_3 films were deposited at low substrate temperature under low oxygen partial pressure [22]. As the substrate temperature increased to 300 °C, the intensities of the cubic peaks were increased while those of the monoclinic peaks were decreased. At temperatures above 300 °C, the monoclinic peak disappeared completely and only the cubic peaks were observed, showing that the films had a single phase of cubic structure. It can also be found from Fig. 5 that the $Y_2O_3:Eu$ films deposited at high temperatures were preferentially oriented along the [111] direction. It is known that the (111) planes have the lowest surface energy in fluorite-derivative oxides [23]. Therefore, it is reasonable that the films having the cubic bixbyite Y_2O_3 structure are textured along the [111] direction.

Figure 6 shows the full width at half maximum (FWHM) of (222) diffraction peak as a function of substrate temperature. The FWHM was decreased as the substrate temperature increased, indicating an improvement in the crystalline quality of the films. This suggests that the $Y_2O_3:Eu$ films deposited at higher substrate temperatures

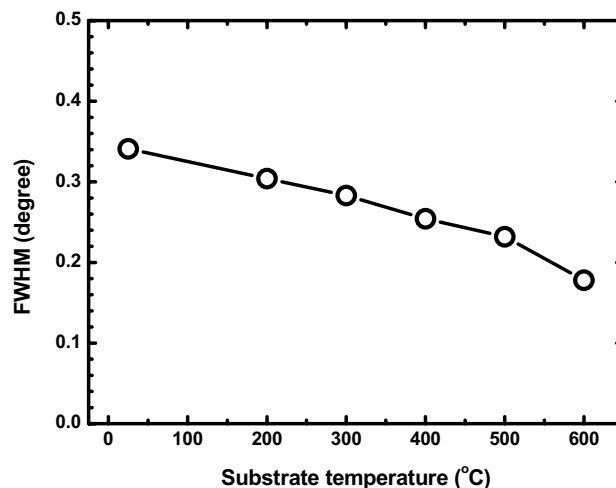


Fig. 6 FWHM of (222) diffraction peak as a function of substrate temperature

have fewer structural defects such as grain boundaries. These defects are known to act generally as non-radiative recombination centers, consequently reducing the luminescence efficiency. It can therefore be found that depositing $Y_2O_3:Eu$ films at higher substrate temperature reduces the

number of the structural defects in the films, thereby leading to higher PL intensity.

Figure 7 shows the residual strain of the films as a function of substrate temperature. The strain (ϵ) value was calculated using the equation, $\epsilon = [(a_{\text{film}} - a_{\text{bulk}})/a_{\text{bulk}}]$, where a_{bulk} is the lattice parameter of bulk Y_2O_3 . It can be found from Fig. 7 that the films were under residual compressive strain, which was decreased with increasing substrate temperature. The observed strain in the films is likely to be intrinsic

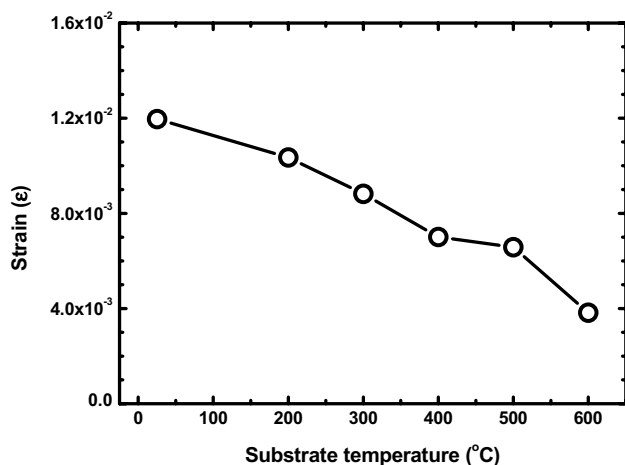
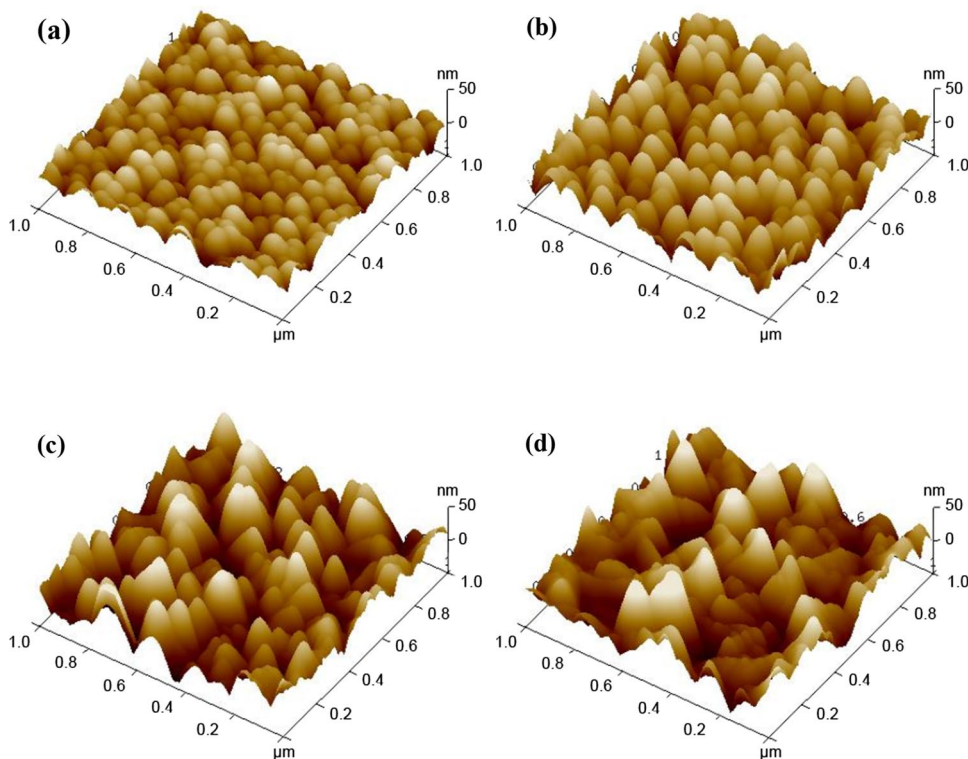


Fig. 7 Residual strain of the $\text{Y}_2\text{O}_3:\text{Eu}$ films as a function of substrate temperature

because the thermal strain induced by the difference between thermal expansion coefficients of the sapphire substrate and the $\text{Y}_2\text{O}_3:\text{Eu}$ film is significantly lower than the measured strain. As substrate temperature increases, atom diffusion is enhanced and structural defects are reduced, resulting in the relaxation of the residual strain in the films. Therefore, the strain in the films decreases with increasing substrate temperature.

Figure 8 shows AFM images of the $\text{Y}_2\text{O}_3:\text{Eu}$ films. As can be seen in Fig. 8a, the $\text{Y}_2\text{O}_3:\text{Eu}$ films deposited at room temperature exhibited a granular surface structure. The grains were uniformly distributed on the surface of the films. As the substrate temperature increased, the grain size was increased and the grain shape changed to a pyramidal faceted structure. Figure 9 shows the surface roughness of the $\text{Y}_2\text{O}_3:\text{Eu}$ films as a function of substrate temperature. It can be seen that the surface roughness was increased as the substrate temperature increased. These AFM results indicate that the crystalline quality of the $\text{Y}_2\text{O}_3:\text{Eu}$ films was improved with increasing substrate temperature. Figure 10 presents the optical transmittance spectra obtained from the $\text{Y}_2\text{O}_3:\text{Eu}$ films deposited at different substrate temperatures. All the films showed good transparency with a transmittance greater than 80% in the wavelength region from 400 to 1100 nm. The films became completely absorbing near 210 nm, indicating an optical absorption edge in deep ultraviolet region. It can be seen that the transmittance of the $\text{Y}_2\text{O}_3:\text{Eu}$ films was decreased as the substrate temperature

Fig. 8 AFM images of the $\text{Y}_2\text{O}_3:\text{Eu}$ films deposited at **a** 25, **b** 300, **c** 500, and **d** 600 °C



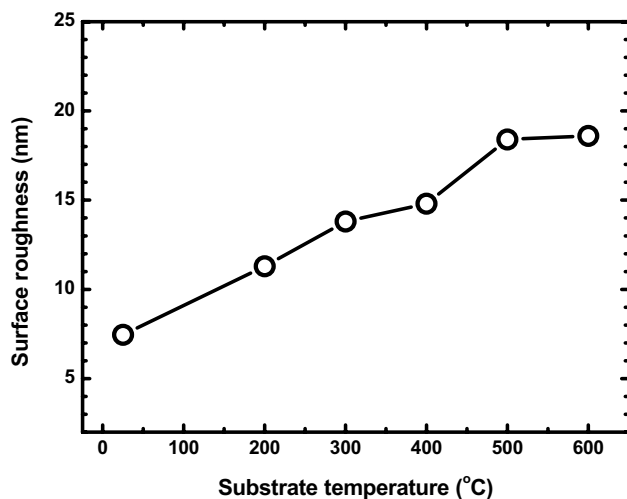


Fig. 9 Surface roughness of the $\text{Y}_2\text{O}_3:\text{Eu}$ films as a function of substrate temperature

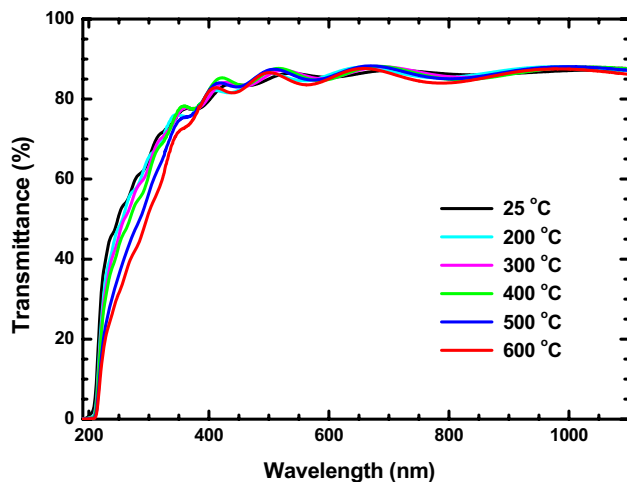


Fig. 10 Optical transmittance spectra obtained from the $\text{Y}_2\text{O}_3:\text{Eu}$ films deposited at different substrate temperatures

increased. This resulted from the increased surface roughness of the films deposited at higher substrate temperatures.

4 Conclusion

We have investigated the structure and luminescence of transparent red-emitting $\text{Y}_2\text{O}_3:\text{Eu}$ thin films deposited at different substrate temperatures. XPS measurements showed that the stoichiometric Y_2O_3 was formed and the Eu ions were incorporated mainly in the form of Eu^{3+} in the films. As the substrate temperature increased, the structure of the $\text{Y}_2\text{O}_3:\text{Eu}$ films changed from a mixed structure of monoclinic and cubic phases to a single phase of cubic structure.

The films deposited at high temperatures were preferentially oriented along [111] direction. The residual compressive strain of the $\text{Y}_2\text{O}_3:\text{Eu}$ films was decreased with increasing substrate temperature. The PL spectra of the $\text{Y}_2\text{O}_3:\text{Eu}$ films consisted of a series of emission peaks with the most intense peak at 613 nm originating from the transition between the $^5\text{D}_0$ and $^7\text{F}_2$ states in Eu^{3+} ions. The PL intensity was increased and the spectral linewidth was decreased with increasing substrate temperature. The $\text{Y}_2\text{O}_3:\text{Eu}$ films exhibited a transmittance greater than 80% in the wavelength region from 400 to 1100 nm. As the substrate temperature increased, the transmittance of the $\text{Y}_2\text{O}_3:\text{Eu}$ films decreased due to the increased surface roughness.

Acknowledgements This work was supported by the National Research Foundation of Korea (NRF) grant funded by the Korea government (MSIT) (No. 2019R1F1A1040480).

References

1. A.L. Costa, A.G. Bispo Jr., S.A.M. Lima, A.M. Pires, J. Alloy. Compd. **843**, 155811 (2020)
2. T.K. Anh, P.T.M. Chau, N.T.Q. Hai, V.T.T. Ha, H.V. Tuyen, S. Bounyavong, N.T. Thanh, L.Q. Minh, J. Electron. Mater. **47**, 585 (2018)
3. H. Wang, M. Uehara, H. Nakamura, M. Miyazaki, H. Maeda, Adv. Mater. **17**, 2506 (2005)
4. J.R. Jayaramaiah, B.N. Lakshminarasappa, K.R. Nagabhushana, J. Lumin. **157**, 63 (2015)
5. A. Sugita, M. Kamiya, C. Morita, A. Miyake, Y. Nawa, Y. Masuda, W. Inami, H. Kominami, Y. Nakanishi, Y. Kawata, Opt. Mater. Express **4**, 155 (2014)
6. A.J. de Morales Ramírez, A. García Murillo, F.J. de Carrillo Romo, J. Ramírez Salgado, C. Le Luyer, G. Chadeyron, D. Boyer, J. Moreno Palmerin, Thin Solid Films **517**, 6753 (2009)
7. M.M. Azrain, G. Omar, M.R. Mansor, S.H.S.M. Fadzullah, L.M. Lim, Opt. Mater. **91**, 85 (2019)
8. Z. Li, H. Meng, *Organic light emitting materials and devices* (CRC Press, Taylor & Francis Group, Boca Raton, FL, USA, 2007)
9. A.M. Shaikh, B.K. Sharma, S. Chacko, R.M. Kamble, RSC Adv. **6**, 94218 (2016)
10. J. Rosa, M.J. Heikkilä, M. Sirkiä, S. Merdes, Materials **14**, 1505 (2021)
11. O.M. Bordun, I.O. Bordun, I.Y. Kukharsky, Z.Y. Tsapovska, M.V. Partyka, J. Appl. Spectrosc. **84**, 1072 (2018)
12. L. Wang, H. Jia, X. Yu, Y. Zhang, P. Du, Z. Xi, D. Jin, Electrochem. Solid-State Lett. **12**, E20 (2009)
13. S.J. Rhee, J.O. White, S. Lee, H. Chen, J. Appl. Phys. **90**, 6110 (2001)
14. K.L. Choy, J.P. Feist, A.L. Heyes, B. Su, J. Mater. Res. **14**, 3111 (1999)
15. G. Gu, P.P. Ong, C. Chen, S. Roth, J. Phys. D: Appl. Phys. **33**, 1263 (2000)
16. J.F. Moulder, W.F. Stickle, P.E. Sobol, K.D. Bomben, *Handbook of X-ray photoelectron spectroscopy* (Physical Electronics, Eden Prairie, MN, USA, 1995)
17. D. Niu, R.W. Ashcraft, G.N. Parsons, Appl. Phys. Lett. **80**, 3575 (2002)
18. X. Zhang, H. Yang, A. Tang, J. Phys. Chem. B **112**, 16271 (2008)

19. G. Beamson, D. Briggs, *High resolution XPS of organic polymers: The Scienta ESCA300 Database* (John Wiley & Sons, Chichester, UK, 1992)
20. Joint Committee on Powder Diffraction Standards (JCPDS), Powder Diffraction Files, Inorganic, No. 43-1036
21. Joint Committee on Powder Diffraction Standards (JCPDS), Powder Diffraction Files, Inorganic, No. 47-1274
22. M.-H. Cho, D.-H. Ko, J.G. Seo, S.W. Whangbo, K. Jeong, I.W. Lyo, C.N. Whangbo, D.Y. Noh, H.J. Kim, *Thin Solid Films* **382**, 288 (2001)
23. G. Ballabio, M. Bernasconi, F. Pietrucci, S. Serra, *Phys. Rev. B* **70**, 075417 (2004)

Publisher's Note Springer Nature remains neutral with regard to jurisdictional claims in published maps and institutional affiliations.